Composites Science and Technology 149 (2017) 220–227

Contents lists available at ScienceDirect

Composites Science and Technology

journal homepage: http://www.elsevier.com/locate/compscitech

# Degradation and recovery of graphene/polymer interfaces under cyclic mechanical loading

Guorui Wang [a, b], Enlai Gao [c], Zhaohe Dai [b], Luqi Liu [b, **], Zhiping Xu [c, ***], Zhong Zhang [b, *]

[a] CAS Key Laboratory of Mechanical Behavior and Design of Materials, Department of Modern Mechanics, University of Science and Technology of China, Hefei 230027, China
[b] CAS Key Laboratory for Nanosystem and Hierarchical Fabrication, National Center for Nanoscience and Technology, Beijing 100190, China
[c] Applied Mechanics Laboratory, Department of Engineering Mechanics and Center for Nano and Micro Mechanics, Tsinghua University, Beijing 100084, China

ARTICLE INFO

*Article history:*
Received 7 April 2017
Received in revised form
6 June 2017
Accepted 8 June 2017
Available online 15 June 2017

*Keywords:*
Graphene
Nano-composites
Dynamic mechanical properties
Degradation
Recovery

ABSTRACT

Interface failure is a common phenomenon for conventional composite materials when subjected to repeated mechanical loads, and it tends to be critical for nanocomposites due to several orders of magnitude enhancement in interfacial area. Herein, the graphene/poly(methyl methacrylate) (PMMA) interface when subjected to cyclic loading conditions exhibits obvious mechanical degradation through interfacial sliding, which has received little attention yet. Through a joint study of experimental tests and molecular dynamics simulations, the interface weakening is attributed to the formation of graphene buckles that not only reduces the interfacial contact area but also impairs the overall interfacial load transfer. However, reminiscent of the shape memory effect that is commonly triggered by temperature, conformational transition at the interfaces exhibits remarkable mechanical recovery under a moderate thermal stimulus, manifested by the interface reconstruction activated by van der Waals (vdW) forces. These findings elucidate the complex interactions between matrix and nanostructures in composite materials under cyclic loading conditions, and control over this mechanism could provide guidelines upon chemical design through tailoring the interfacial adhesion for specific applications.



## 1. Introduction

Nanostructured carbon material based composites, typically reinforced with carbon nanotubes (CNTs) and graphene nanosheets, are currently the subject of extensive worldwide research for their promising applications as light-weight and multifunctional components. Apart from the static mechanical loading conditions, these composite materials are frequently subjected to cyclic loads or structural vibrations for both scientific and industrial applications, such as artificial muscles [1] and internal sensors in aircraft structures or wind blades [2]. Earlier works have revealed the varied failure modes in fiber reinforced composites when subjected to long-term cyclic loads [3–6]. For instance, apparently degraded interfacial shear stress was observed in fiber reinforced composites after experiencing several tens of loading cycles [5]. Given the fact that interface plays a critical role in the macroperformance of fiber reinforced composites, a comprehensive knowledge of interface behaviors under cyclic loading and unloading modes is essentially important for durability and reliability of composites. Furthermore, the impact of interface becomes much more notable on the mechanical performance of nanostructured carbon material based composites, since the interfacial area is at least several orders of magnitude greater than that of traditional fiber reinforced composites with the same volume fraction. However, limited by the tiny size of nanofiller itself, the micromechanical test methods in conventional fiber based composites (e.g. fiber pullout, fragmentation, and micro-debonding test) cannot be directly employed to measure the interfacial properties in nanostructured carbon material based composites.

Owing to the stress-sensitive characteristics of specific Raman peaks of nanostructured carbon materials, in situ Raman spectroscopy has become a powerful tool to monitor the interfacial shear stress transfer, strain distribution and deformation modes at a microscopic level [7–14]. Our earlier works have revealed the

* Corresponding author.
** Corresponding author.
*** Corresponding author.
*E-mail addresses:* liulq@nanoctr.cn (L. Liu), xuzp@tsinghua.edu.cn (Z. Xu), zhong.zhang@nanoctr.cn (Z. Zhang).

http://dx.doi.org/10.1016/j.compscitech.2017.06.004
0266-3538/

dependence of load-bearing capability of nanotubes on the interfacial couplings at molecular level for CNTs reinforced composites. A strain transfer factor was proposed to quantify the strain transfer efficiency from macroscale strain to axially strained individual nanotubes [14]. Technically, however, it is hard to directly derive the interfacial shear strength between nanotubes and adjacent polymer matrix due to nanoscale diameter of single nanotube. Instead, the microscale lateral dimension of individual graphene sheets made it possible to monitor the shear stress transfer at different applied strain levels, and then derive interfacial shear strength for monolayer graphene/polymer composite system [7,10]. Several works have shown the interfacial shear strength values ranged from 0.3 to 0.8 MPa for van der Waals (vdW) forces dominated graphene/polymer interface. Recently, we introduced hydrogen bonding at graphene/PMMA interface, and apparent enhancement of interfacial shear strength up to 1.7 MPa was achieved [15,16]. Meanwhile, on the basis of the varied trend of strain profiles in response to external strain, the interfacial sliding, interfacial debonding as well as buckling were characterized in the graphene based composites. To date, even the great achievement has been achieved in the interfacial mechanical behaviors of nanostructured carbon materials based composites under static loads, a thorough understanding of the interfacial mechanical behaviors under cyclic loads have not been explored yet.

In this work, in situ Raman spectroscopy was employed to monitor the interfacial stress transfer process and reveal the possible deformation modes of graphene/PMMA interface when subjected to cyclic loading and unloading. Meanwhile, AFM was utilized to characterize the variation of morphology of monolayer graphene sheet before and after each loading and unloading cycle. Our results unveil an unusual interfacial behavior at nanoscale interface, where apparently degraded interfacial shear stress transfer was observed during short-term loading/unloading cycles. That could be attributed to the formation of graphene buckles during the unloading process, as evidenced by AFM characterization and molecular dynamics (MD) simulations. Surprisingly, the buckled structures and degraded interfacial properties could be recovered under moderate thermal stimulus, which haven't been achieved in conventional composites. Our works provide valuable insights into the fundamental interfacial mechanics at nanoscale driven by vdW interaction, and shed light on tailoring mechanical behaviors of the interface itself for specific applications with superior mechanical performance.

## 2. Experimental section

### 2.1. Sample preparation

The graphene samples were prepared by micromechanical cleavage [22] and then deposited onto the Si wafer substrate with a 300 nm $SiO_2$ capping layer. Optical microscopy was used to locate the graphene sheet and the corresponding thickness was further confirmed by Raman spectroscopy and atomic force microscopy (AFM). AFM images were recorded using a Dimension 3100 Veeco in the Peak Force tapping mode. Using the same method as reported in our earlier work, the monolayer graphene sheet was then successfully transferred onto the surface of PMMA bar [23]. It should be noted that, instead of embedding graphene sheet inside PMMA matrix, the monolayer graphene sheet was exposed on top of a PMMA beam in this work, which would facilitate the morphology characterization of graphene sheet before and after deformation.

### 2.2. In situ tensile and micro Raman spectroscopy tests

Mechanical deformation of the PMMA cantilever beam is applied by mounting it onto a piezoelectric stage with a spatial resolution of 600 nm in the Renishaw Raman spectroscope setup, as shown in Fig. 1a. The tensile strain within the individual graphene sheet deposited onto the top surface of the beam is given by Equation (1) [24].

$$\varepsilon\left(x, \frac{t}{2}\right) = \frac{3t\delta(L - x)}{2L^3} \quad (1)$$

where $x$ is the location in graphene sheet measured from the fixed end of beam, $t$ is the thickness of the beam, $L$ is the span of the beam and $\delta$ is the deflection of loading point at the other end of beam, as shown in Fig. 1a. To make the assumptions for Equation (1) valid, experimentally, the aspect ratio of span at maximum deflection was ensured to be higher than 10, and the in-plane strain in graphene was within the range from −1.5% to +1.5% [25]. Remarkably, bending of the cantilever beam would lead to a strain gradient on the top surface, but herein, the strain variation across the graphene flake (along the $x$ direction) was actually less than 0.005% at a given strain level of 1%, that is attributed to the limited span of graphene flake (~10 μm). Consequently, tensile strain within the flake could be regarded as a constant for the estimation of the strain level. The tensile strain was applied with an increment step of ~0.05%. All bands in the Raman spectra of graphene were recorded using the 514.5 nm line of an Ar laser and fitted with Lorentzians. To obtain the strain distribution based on the line profile of Raman 2D-band frequency, the graphene sheet under measurement was moved with a step size of 600 nm and the Raman spectra from every spot of the sample was recorded.

### 2.3. Coarse-grained molecular dynamics

As full-atom MD simulations cannot access the length scale and the corresponding time scale of current system, a coarse-grained molecular dynamics (CGMD) approach was pursued here. This approach provides an energetic description equivalent to the continuum mechanics model with specific tensile stiffness, Poisson's ratio, bending rigidity and the adhesion between graphene and the PMMA substrate. All simulations were performed by using the large-scale atomic/molecular massively parallel simulator (LAMMPS) package [26]. Detailed information is presented in Supporting Information S1.

## 3. Results and discussion

The graphene samples were prepared by micromechanical cleavage and deposited onto the silicon wafer substrate, as shown in the left inset of Fig. 1a. Then, the exfoliated graphene flakes were transferred onto a PMMA cantilever beam and mechanically loaded with uniaxial tension by bending the beam following our previous strategy, as illustrated in Fig. 1a [15]. Such a film/substrate setup also allows surface morphology characterization of the graphene sheet before and after bending the substrate, as demonstrated by the AFM image (Fig. 1a, right inset). Raman spectra in Fig. 1b display characteristic peaks (G-band and 2D-band) for monolayer graphene both on silicon and PMMA substrates. It is obvious that the perfect lattice structure is maintained for exfoliated graphene flakes, featuring the absence of Raman D-band (black curve) [27]. The transfer process was also successful without introducing any defects or damages, despite of two additional Raman peaks

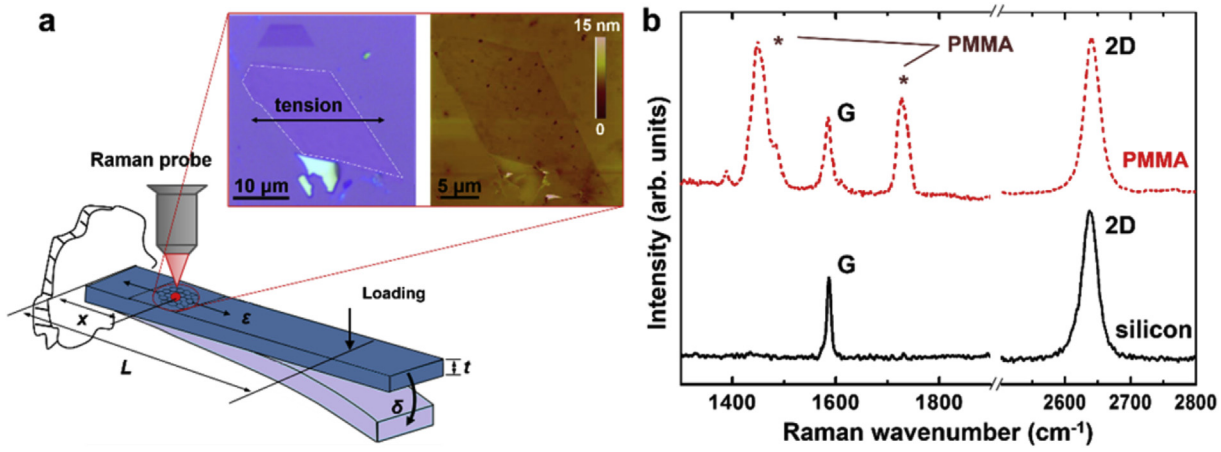


**Fig. 1.** (a) The schematic diagram of PMMA cantilever beam that transfers bending to monolayer graphene samples. The optical (the left panel) and AFM images (the right panel) of the graphene sheet are shown as the insets. (b) Raman spectra of monolayer graphene deposited onto silicon and PMMA substrates.

originated from the PMMA substrate (red curve). In this work, the Raman 2D-band of monolayer graphene sheet was in situ recorded at different strain levels during loading due to its high intensity as well as higher strain sensitivity (~−49 $cm^{-1}$/%) compared to that of the Raman G-band (~−30 $cm^{-1}$/%) [10].

### 3.1. Interfacial stress transfer during loading and unloading

Raman spectroscopy has been successfully employed to measure the in-plane strain in graphene due to the high sensitivity of Raman shifts to follow the evolution of strain [7,8,11,28]. Fig. 2a presents the evolution of the Raman 2D-band recorded at the center of monolayer graphene flake, in response to the bending deformation. The two-stage features are clearly exhibited, as further summarized in Fig. 2b. During the bending deformation process, initially, the Raman 2D-band displays a linear downshift up to 0.7% with a rate of −49 $cm^{-1}$/%, followed by a plateau with further increasing strain. The initial linear stage is correlated to the elastic stress transfer from substrate to graphene sheet, and then followed by the occurrence of interfacial sliding evidenced by a plateau stage [10]. Once the bending load is released, the peak position upshifts accordingly at a rate of −51 $cm^{-1}$/% and remain as a constant at the end of unloading. Similar Raman peak shift was also observed in the PMMA/graphene/SU8 (−60 $cm^{-1}$/%) and graphene/polyethylene terephthalate (PET) systems (−52.5 and −49.4 $cm^{-1}$/%) [7,10,29]. Conceivably, the graphene sheet tends to recover to its initial state with Raman 2D-band located at ~2690 $cm^{-1}$ as the strain is reduced to 0.4%. Further continuous release would cause slight compression as well as interfacial buckling (more details in following discussion) supported by the relatively higher peak positions (~2695 $cm^{-1}$) at the plateau.

To gain a deep understanding of the interfacial stress transfer from the PMMA substrate to graphene, and reveal the possible failure modes at the graphene/PMMA interface, a nonlinear shear-lag model was adopted here as reported in our previous works [16]. Briefly, the interfacial sliding behavior between graphene and PMMA substrate during uniaxial tension can be described by the relationship between the shear traction ($\tau$) and sliding displacement ($\delta$) [30]. As can be seen in Fig. 2c, in the elastic stage, shear traction first increases linearly in response to the sliding displacement until reaching the interfacial shear strength ($\tau_s$). Beyond the elastic stage, there is a shear sliding stage with the sliding stress assumed to be constant at $\tau_s$ while the sliding displacement further increases, agreeing well with our experimental results in Fig. 2b. This plateau is stemmed from the breaking and re-forming nature of vdW interactions to maintain the stress transfer during the shear sliding [31–33]. Accordingly, at low strain levels (e.g. $\varepsilon_m < 0.2\%$), the whole length of interface is in elastic conditions and the strain distribution could hence be fitted by Equation (2):

$$\varepsilon_g = \varepsilon_m \left[1 - \frac{\cosh(\beta x)}{\cosh(\beta L/2)}\right] \tag{2}$$

where $L$ is the length of graphene flake along in the $x$ direction with the center located at $x = 0$, and $\beta$ is the shear-lag parameter which is typically treated as an effective measure for the efficiency of interfacial stress transfer [10]. From Fig. 2d it can be seen that strain builds up in graphene sheet from the edges along the $x$ direction, and approaches a peak at the center, which is approximately equal to the strain in the matrix. The strain distribution of graphene sheet could be well described by Equation (2) with $\beta L = 10$ (solid lines). Once sliding stress reaches the interfacial shear strength, interfacial sliding occurs. Correspondingly, the sliding zone develops from both edges of the sheet, approaches the center gradually as the loading amplitude increases. Eventually, the strain at center in graphene saturates at a constant level as we observed in Fig. 2d. Meanwhile, in the sliding zone, the in-plane strain distribution in graphene becomes almost linear and tends to be in a triangle-like shape near the edges. The interfacial shear strength at the graphene/PMMA interface can be estimated by fitting the slope of this sliding-induced in-plane strain distribution through following equation:

$$\tau_s = Et\frac{d\varepsilon}{dx} \tag{3}$$

with known parameters including the Young's modulus $E = 1$ TPa and thickness $t = 0.34$ nm of graphene. In our work, the obtained value is ~0.5 MPa, coinciding well with the results reported previously for PMMA/graphene/SU8 (0.3–0.8 MPa) and graphene/PET (0.7 MPa) laminates [7,10].

### 3.2. Degradation of interfacial stress transfer during cyclic loading

We further conduct cyclic loading/unloading tests to the graphene/PMMA composite system through applying and releasing the bending load to the cantilever. Herein, the applied strain level is increased up to 0.7% to ensure the occurrence of interfacial sliding at the center of graphene sheet, and thus a triangle-like shaped

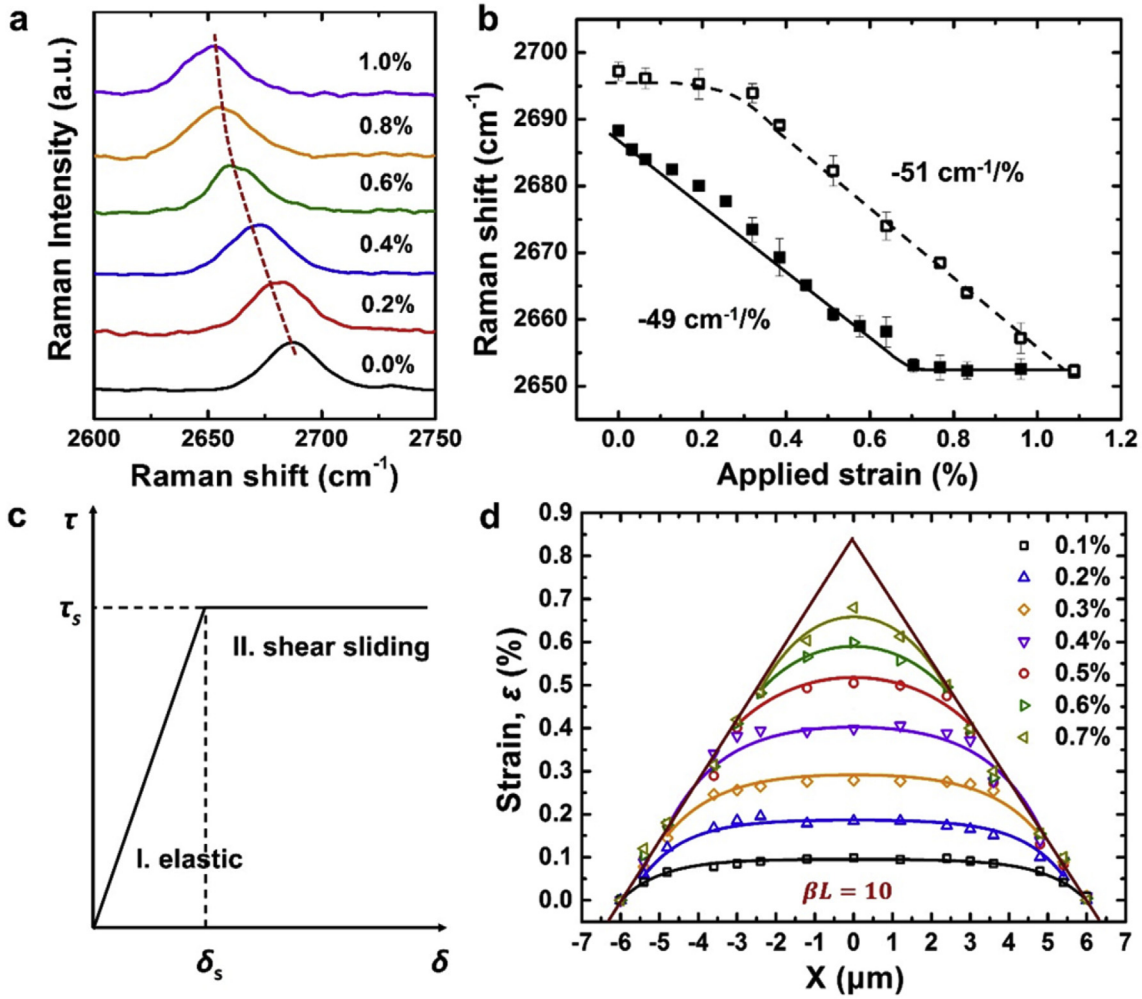


**Fig. 2.** (a) Evolution of the Raman 2D spectrum for graphene with increasing applied strain. (b) Raman 2D-band shifts during a loading/unloading cycle. Raman 2D band were recorded at the center of monolayer graphene flake. (c) Shear traction ($\tau$)-sliding displacement ($\delta$) relationship from the nonlinear shear-lag model. (d) Strain distribution in the direction of stretching axis of graphene sheet at different strain levels.

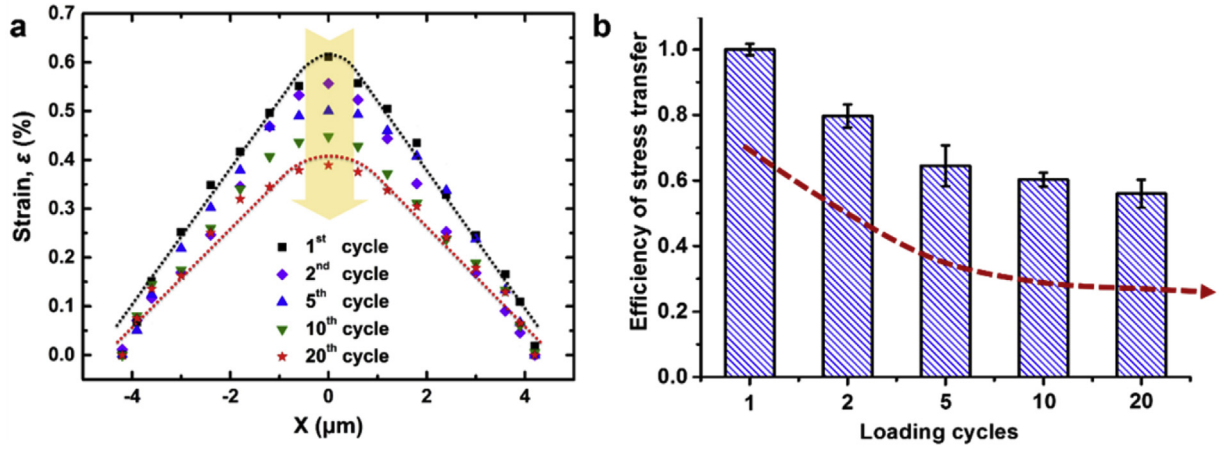


**Fig. 3.** (a) Strain distribution in the direction of stretching axis of graphene sheet at the strain level of 0.7% in multiple loading/unloading cycles. (b) Variation of the efficiency of stress transfer with increasing loading cycles.

strain distribution is expected. As shown in Fig. 3a, once the graphene sheet was subjected to multiple loading/unloading cycles, the slope of the strain gradient ($\frac{d\varepsilon}{dx}$) exhibits an obvious decreasing tendency, corresponding to the weakened efficiency of shear stress transfer. Specifically, for 1st loading process, $\frac{d\varepsilon}{dx}$ is approximated to

0.14%/μm, while at 20th loading cycles, $\frac{d\varepsilon}{dx}$ is reduced to 0.09%/μm. To quantify the efficiency of shear stress transfer across interface at different loading cycles, the ratios of $\frac{d\varepsilon}{dx}$ at a given cycle is normalized to that of at 1st cycle. Fig. 3b summarizes weakening trend of stress transfer efficiency during the twenty loading/unloading cycles, and a plateau is expected to further increase loading/unloading cycles. Such apparently decreased values imply the interface degradation once subjected to cyclic loads, which has not been considered in previous studies [9,34].

To gain more insights into the underlying degradation of interfacial shear stress transfer, AFM images were recorded to monitor the evolution of surface morphology of graphene sheet after each loading/unloading cycle. Herein, to quantitatively describe the surface morphology, the surface roughness as the most widely used roughness parameter was introduced, defined as $R_a = \frac{1}{n}\sum_{i=1}^{n}|y_i|$, where $y_i$ is the vertical distance from the mean line to the $i^{th}$ data point in the AFM image. As shown in Fig. 4a, the graphene sheet is relatively flat with an average roughness of ~0.4 nm before the load is applied (calculated by the Nanoscope software). After the first loading/unloading cycle with tensile strain of 0.7% (to ensure strain at the center of graphene sheet could reach a plateau), the graphene sheet demonstrates randomly distributed buckles as shown in Fig. 4b. Correspondingly, the surface roughness of individual graphene sheet increases to ~1.73 nm. It is conceivable that the formation of buckles is related to the mechanical compression during unloading process, as discussed in Fig. 2b and further detailed in Fig. S1. It is worth noting that, different from the regular surface morphology with periodic buckles in response to the uniaxial compression in most systems [35,36], the formation of buckles with random orientation here could be attributed to the Poisson's ratio effect during the loading/unloading cycles, as well as the influence of geometry and orientation of individual graphene sheets with respect to the loading axis [17,18]. Compared with the 1st cycle, we find that the amplitudes of buckles tend to increase in the 2nd loading/unloading cycle as presented in Fig. S2. Accordingly, the surface roughness also increases to ~2.05 nm. With further bending and releasing cycles up to the 5th (Fig. 4d), the amplitudes of buckles grow continuously together with the enhancement of averaged surface roughness ~3.08 nm (Fig. 4i). After 20th loading/unloading cycles, merely slight increase in amplitudes could be observed and the corresponding surface roughness is improved to ~3.24 nm. This sluggishly increased tendency is in good agreement with the plateau stage following the degradation of interfacial shear stress presented in Fig. 3b. We suggest that the formation of buckles with nanoscale height and width after mechanical loading/unloading might break the full contact between graphene and PMMA into patches. As a result, the decreased contact area at graphene/PMMA interface would impair interfacial adhesion, and eventually result in the degradation of interfacial stress transfer in the graphene/polymer system.

To validate aforementioned deformation mechanisms of nanoscale interface, MD simulations were performed to clarify the interface degradation during cyclic loading and unloading. Similar to AFM image shown in Fig. 4a, initially, the monolayer graphene appears flat and keeps a relatively full contact with the supporting PMMA substrate as shown in Fig. 5a. Then, the graphene sheet is strained through shear stress across graphene/PMMA interface at a constant rate of $8 \times 10^8$ $s^{-1}$. The interfacial sliding occurs as the matrix strain is higher than 3%, and then the average strain in graphene would step into a plateau region. Meanwhile, the shear stress reaches $\tau_s$ and the interfacial stress transfer is governed by interfacial sliding [10]. It should be emphasized here that due to the discrepancy of graphene sheet sizes in simulation and experimental setups (~40 nm vs ~10 μm), the absolute strain level in graphene would be different. Upon unloading, the strain in graphene drops immediately, even down to the negative value, implying the subtle compressive strain it bears. Consequently, the graphene sheet tends to buckle to release the compressive strain energy. In contrast to the AFM characterizations showing buckling of graphene in a networked pattern due to the Poisson's ratio effect, herein, MD simulation only focuses on revealing the mechanism along the length direction, and the width of graphene in molecular model is far smaller than that in experiments considering computational consumption, which limits the buckling behavior in width direction. The weakened interfacial adhesion and efficiency of shear stress transfer are expected due to the reduced interfacial contact area during the subsequent loading cycles. Fig. 5b summarizes the variation of average strain in graphene and the interfacial adhesion energy over three cycles. In the 2nd and 3rd loading/unloading cycles, both the average strain in graphene and the interfacial adhesion energy degrade apparently due to interfacial sliding and the subsequent buckles induced by compression.

To deeply understand the effect of graphene buckles on the mechanical performance of composites, we employ a nonlinear shear-lag model to quantitatively evaluate the efficiency of shear stress transfer. As known that the critical length ($l_c$) of fillers is one of major factors to determine the mechanical reinforcement, and at

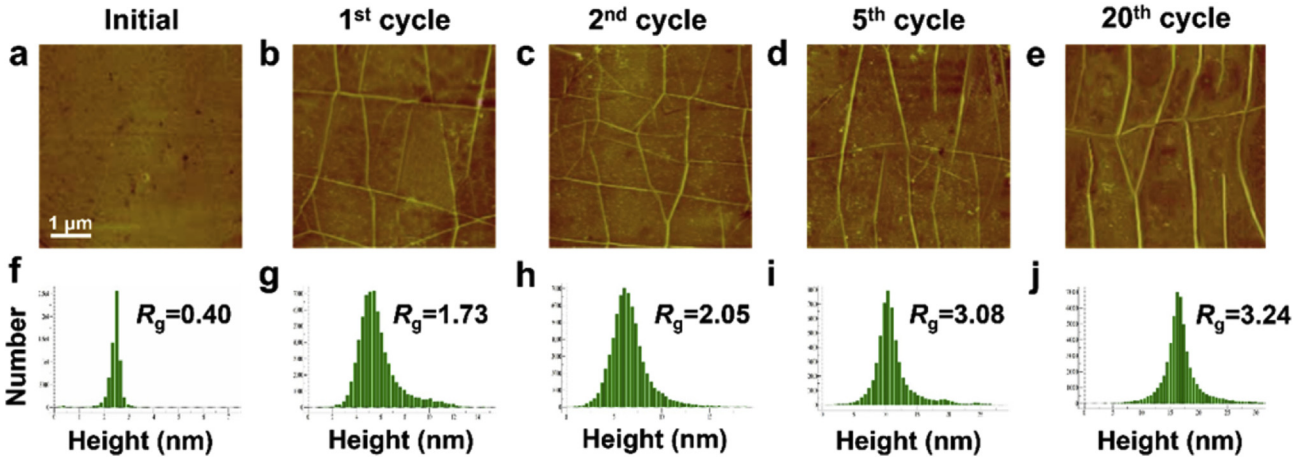


**Fig. 4.** (a–e) AFM images of the graphene sheet deposited on PMMA, which is subjected to twenty cycles of loading and unloading. The images were recorded from the same flake whereas the scanning area might slightly deviate from each other. The evolution of its morphology is demonstrated by the variation of roughness distribution as presented in (f–j).

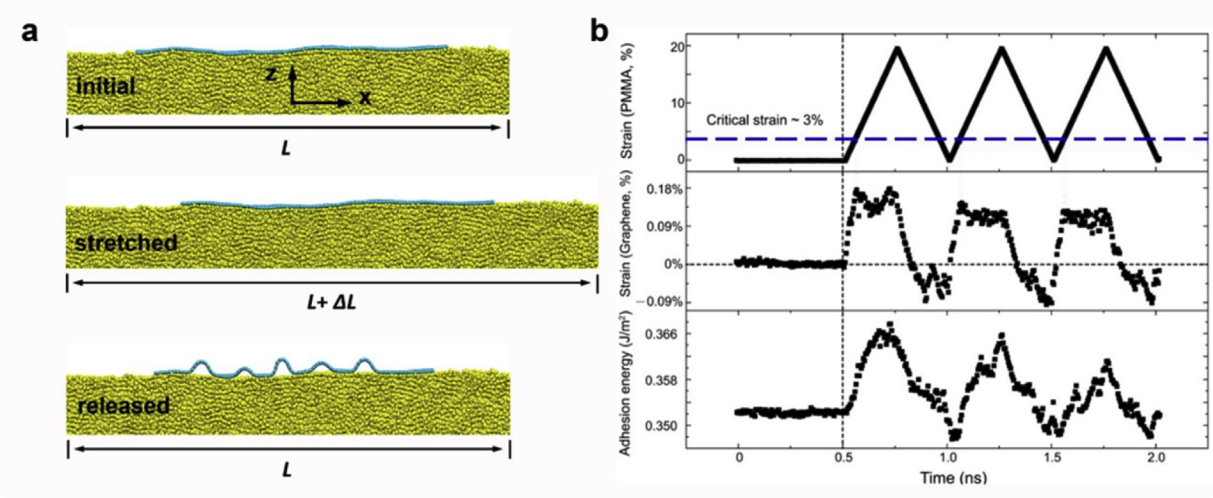


**Fig. 5.** (a) Simulation snapshots that illustrate the morphological changes of graphene from a flat sheet fully in contact with the substrate to a series of partial contact separated by buckles formed due to the compression-induced buckling upon unloading. (b) The evolution of strain in the substrate, graphene and their interfacial adhesion energy as a function of time.

least twice length is required to reach 90% of the matrix strain [7,19]. Here, we define the efficiency of stress transfer $\eta = 1 - \frac{tanh(\beta L/2)}{\beta L/2}$ by the ratio of the integral area of $\varepsilon(x)$ to the rectangular area surrounded by dashed lines and coordinate axes as shown in bottom panel of Fig. S3a. For instance, a monolayer graphene with lateral span of $L = 15$ μm along the stretching direction ($x$), the derived fitting parameter is $\beta L = 10$ (detail in Fig. 2d), thus we have $\eta = 0.80$ for full contact graphene/PMMA interface. After first loading/unloading cycle, the pristine full contact between graphene and substrate is broken into a series of patches, and the buckles tend to stretch straightly instead of transfer stress transfer. As shown in Fig. 4c, for the graphene/PMMA interface with buckled morphologies (the width of patches is ~1.5 μm in average based on AFM characterization), $\eta$ would decrease to ~0.55, suggesting significantly reduced overall efficiency of interfacial stress transfer. Even the limited spatial resolution of Raman spectroscopy (~1 μm) hinders us from directly visualizing such variation in terms of strain distribution of the stretched graphene, the theoretical analysis together with MD simulations offers straightforward evidence upon the combined effect of reduced contact area and decreased interfacial adhesion which is responsible for the observed degradation of stress transfer at the graphene/PMMA interface.

It is worth noting that, to circumvent the difficulties in experimental observations of graphene incorporated in a polymer matrix, herein, graphene flakes were directly deposited on the surface of the polymer substrate with only one interface. However, additional constraints from two sides of graphene in the nanocomposite are expected to cause different mechanical responses, especially the graphene/polymer interfacial properties. For instance, the above-mentioned buckling formed during cyclic loadings could be effectively suppressed when the graphene is fully embedded in a polymer matrix so that the degradation tends to be mitigated. Herein, we merely attempt to clarify the underlying mechanism of degradation at graphene/polymer interface that is similar for both uncoated (one interface) and coated (two interfaces) model composite specimens.

### 3.3. Recovery of interfacial properties in graphene/polymer system

The poor contact between graphene and substrate caused by compression induced buckles could result in the apparent degradation of interface performance. Inspired by the shape memory effect of polymeric materials that is the stimuli-responsive control of transition between metastable morphologies, we employ thermal treatment to modulate the buckled morphologies of graphene sheet [20]. AFM images were recorded to characterize the variation of graphene morphologies before and after mechanical and thermal treatment. Fig. 6a presents two individual graphene sheets with ribbon and triangle-like shapes with several buckles parallelized to each other within the relatively flat graphene sheets. The presence of buckles was attributed to the residual strain during graphene sheets transfer process [11,21]. After twenty loading/unloading cycles, the randomly oriented new buckles are formed as shown in Fig. 6b. The amplitudes of buckles are similar to the previous ones as presented in Fig. 4, approximated to 6.8 nm, while much lower than those of pre-exist buckles (~23.2 nm). Once the thermal treatment was applied to the sample (at ~40 °C for a week), the enhanced mobility of polymer chains under thermal stimuli would facilitate the flattening of graphene and hence relaxation of buckles (Fig. 6c). Meanwhile, we notice that the thermal stress applied to the graphene sheet could be neglected, where the negligible difference (3 $cm^{-1}$) in the Raman 2D band frequency before and after thermal treatment was observed (Fig. S4).

To experimentally validate the recovery of the interfacial interaction, cyclic mechanical tests were applied to the same specimen. The strain distribution of graphene sheet at various strain levels exhibit the similar triangle-like shape features shown in Fig. S5. Herein, we name the first degradation/recovery cycle as a Test I as shown in Fig. 6d, which suffered twenty loading/unloading cycles and followed by thermal treatment. Obviously, the efficiency of shear stress transfer extracted from Test II almost recover to the initial value, and then exhibits the similar decreasing tendency in the subsequent loading/unloading cycles. Additionally, the same shear stress transfer behaviors are observed in the Test III.

To explore the reconstruction of graphene/PMMA interfacial interaction under thermal stimuli in molecular simulation, a three-cycle loading condition was simulated at ultra-low temperature (0 K) as the system in simulation is more sensitive to thermal fluctuation than that in experiments. As a result, obvious buckle configurations and relatively larger reduction of strain in graphene are observed in Fig. 6e. After three-cycle loading, thermal stimulus of 300 K heating up is introduced to the system, and the strain in

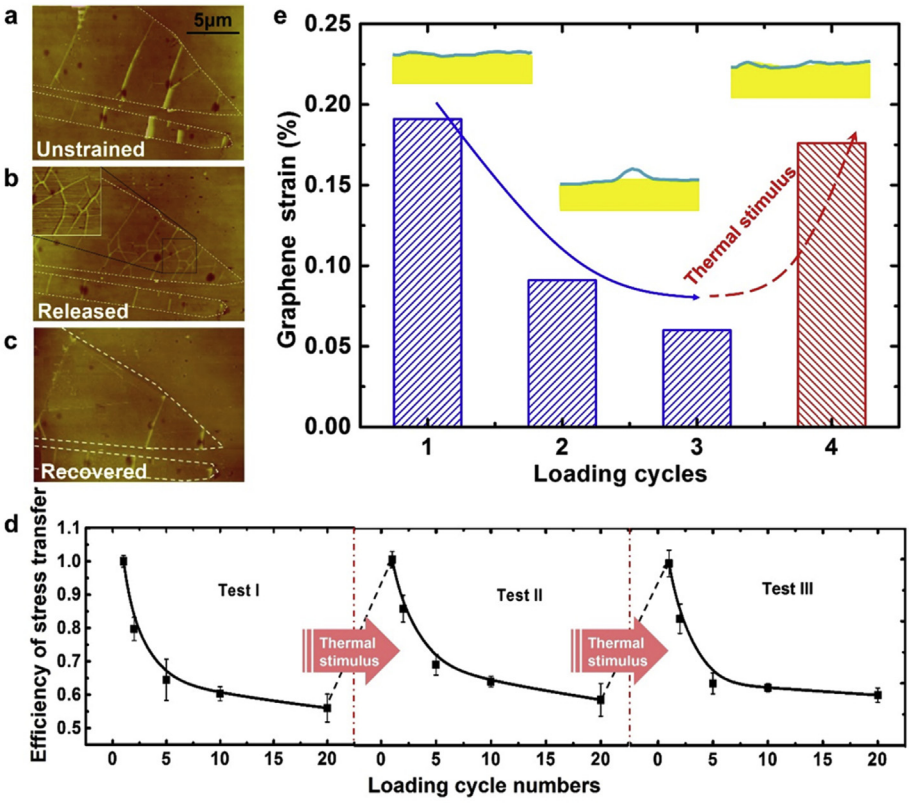


**Fig. 6.** (a–c) AFM images of graphene before (a), after (b) cycling loads, and after thermal treatment (c). (d) The recovery of the average strain in graphene by the thermal stimulus. Insets are simulation snapshots of a graphene sheet deposited on to the PMMA substrate in the unstrained, released and recovered states, respectively. (e) The recovery of degraded interfacial stress transfer triggered by thermal stimuli.

graphene can be remarkably recovered through thermally activated interfacial sliding that heal the buckles, with a reconstructed interfacial morphology and interaction. Interestingly, the recovered interfacial performance in the graphene/PMMA composites is apparently different from that of in conventional fiber reinforced composites. We expect that the observed degradation of interfacial behavior of graphene/polymer system is likely to happen for stretchable electronic devices over their lifetime when subjected to cyclic deformation. Therefore, thermal stimuli activated mechanical recovery at the interface tends to be an effective route for the interfacial recovery and long-time service of stretchable electronic devices.

## 4. Conclusion

We have demonstrated that a combination of in situ Raman spectroscopy technique and AFM measurements offers a thorough insight into the dynamic behaviors of graphene/PMMA interface. The interfacial shear stress transfer between graphene and the PMMA matrix, monitored via strain-dependent shifts of 2D-Raman bands, displays a decreasing tendency during multiple loading/unloading cycles, which is possibly relevant to the formation of buckles in graphene during repeated deformations. The underlying mechanisms lie in not only the impaired contact and hence adhesion at graphene/PMMA interface as verified by the molecular simulations, but also the reduced efficiency of interfacial stress transfer due to the formation of graphene patches separated by buckles according to the nonlinear shear lag analysis. With a thermal stimulus imposed on the specimen, the mechanical recovery of the interface is achieved, as evidenced by the final disappearance of distributed buckles in graphene. Our observations on the interfacial mechanics between graphene and the polymer matrix would enable mechanically stable graphene-based nanocomposites, and offer valuable insights into tailoring behaviors of nanoscale interfaces for specific applications.

## Acknowledgements

This project was jointly supported by the National Key Basic Research Program of China (Grant No. 2013CB934203 and 2012CB937503) and the National Natural Science Foundation of China (Grant Nos. 21474023 and 11225210).

## Appendix A. Supplementary data

Supplementary data related to this article can be found at http://dx.doi.org/10.1016/j.compscitech.2017.06.004.

## References

[1] Z. Dai, Y. Wang, L. Liu, X. Liu, P. Tan, Z. Xu, J. Kuang, Q. Liu, J. Lou, Z. Zhang, Hierarchical graphene-based films with dynamic self-stiffening for biomimetic artificial muscle, Adv. Funct. Mater. 26 (38) (2016) 7003–7010.
[2] A. de la Vega, J. Sumfleth, H. Wittich, K. Schulte, Time and temperature dependent piezoresistance of carbon nanofiller/polymer composites under dynamic load, J. Mater. Sci. 47 (6) (2011) 2648–2657.
[3] C.D. Cho, J.W. Holmes, J.R. Barber, Estimation of interfacial shear in ceramic composites from frictional heating measurements, J. Am. Ceram. Soc. 74 (11) (1991) 2802–2808.
[4] R. Brighenti, A. Carpinteri, D. Scorza, Micromechanical model for preferentially-oriented short-fibre-reinforced materials under cyclic loading, Eng. Frac. Mech. 167 (2016) 138–150.
[5] A. Evans, F. Zok, R. McMeeking, Fatigue of ceramic matrix composites, Acta Metall. Mater. 43 (3) (1995) 859–875.

[6] A. Pupurs, S. Goutianos, P. Brondsted, J. Varna, Interface debond crack growth in tension-tension cyclic loading of single fiber polymer composites, Compos. Part A 44 (2013) 86–94.
[7] L. Gong, I.A. Kinloch, R.J. Young, I. Riaz, R. Jalil, K.S. Novoselov, Interfacial stress transfer in a graphene monolayer nanocomposite, Adv. Mater. 22 (24) (2010) 2694–2697.
[8] R.J. Young, L. Gong, I.A. Kinloch, I. Riaz, R. Jalil, K.S. Novoselov, Strain mapping in a graphene monolayer nanocomposite, ACS Nano 5 (4) (2011) 3079–3084.
[9] A.P.A. Raju, A. Lewis, B. Derby, R.J. Young, I.A. Kinloch, R. Zan, K.S. Novoselov, Wide-area strain sensors based upon graphene-polymer composite coatings probed by Raman spectroscopy, Adv. Funct. Mater. 24 (19) (2014) 2865–2874.
[10] T. Jiang, R. Huang, Y. Zhu, Interfacial sliding and buckling of monolayer graphene on a stretchable substrate, Adv. Funct. Mater. 24 (3) (2014) 396–402.
[11] O. Frank, G. Tsoukleri, J. Parthenios, K. Papagelis, I. Riaz, R. Jalil, K.S. Novoselov, C. Galiotis, Compression behavior of single-layer graphenes, ACS Nano 4 (6) (2010) 3131–3138.
[12] C. Xu, T. Xue, J. Guo, Q. Qin, S. Wu, H. Song, H. Xie, An experimental investigation on the mechanical properties of the interface between large-sized graphene and a flexible substrate, J. Appl. Phys. 117 (16) (2015) 164301.
[13] W. Ma, L. Liu, R. Yang, T. Zhang, Z. Zhang, L. Song, Y. Ren, J. Shen, Z. Niu, W. Zhou, S. Xie, Monitoring a micromechanical process in macroscale carbon nanotube films and fibers, Adv. Mater. 21 (5) (2009) 603–608.
[14] W. Ma, L. Liu, Z. Zhang, R. Yang, G. Liu, T. Zhang, X. An, X. Yi, Y. Ren, Z. Niu, J. Li, H. Dong, W. Zhou, P.M. Ajayan, S. Xie, High-strength composite fibers: realizing true potential of carbon nanotubes in polymer matrix through continuous reticulate architecture and molecular level couplings, Nano Lett. 9 (8) (2009) 2855–2861.
[15] G. Wang, Z. Dai, L. Liu, H. Hu, Q. Dai, Z. Zhang, Tuning the interfacial mechanical behaviors of monolayer graphene/PMMA nanocomposites, ACS Appl. Mater. Interfaces 8 (34) (2016) 22554–22562.
[16] Z. Dai, G. Wang, L. Liu, Y. Hou, Y. Wei, Z. Zhang, Mechanical behavior and properties of hydrogen bonded graphene/polymer nano-interfaces, Compos. Sci. Technol. 136 (2016) 1–9.
[17] A.K. Geim, K.S. Novoselov, The rise of graphene, Nat. Mater. 6 (3) (2007) 183–191.
[18] G. Wang, L. Liu, Z. Dai, Q. Liu, H. Miao, Z. Zhang, Biaxial compressive behavior of embedded monolayer graphene inside flexible poly (methyl methacrylate) matrix, Carbon 86 (2015) 69–77.
[19] S. Timoshenko, J.M. Gere, Theory of Elastic Stability, Dover Publications. com, 2012. Chap. 1.
[20] M.G. Dobb, D.J. Johnson, C.R. Park, Compressional behavior of carbon-fibers, J. Mater. Sci. 25 (2A) (1990) 829–834.
[21] S. Plimpton, Fast parallel algorithms for short-range molecular-dynamics, J. Comput. Phys. 117 (1) (1995) 1–19.
[22] A.C. Ferrari, J.C. Meyer, V. Scardaci, C. Casiraghi, M. Lazzeri, F. Mauri, S. Piscanec, D. Jiang, K.S. Novoselov, S. Roth, A.K. Geim, Raman spectrum of graphene and graphene layers, Phys. Rev. Lett. 97 (18) (2006) 187401.
[23] C. Xu, T. Xue, J. Guo, Y. Kang, W. Qiu, H. Song, H. Xie, An experimental investigation on the tangential interfacial properties of graphene: size effect, Mater. Lett. 161 (2015) 755–758.
[24] G. Guo, Y. Zhu, Cohesive-shear-lag modeling of interfacial stress transfer between a monolayer graphene and a polymer substrate, J. Appl. Mech. 82 (3) (2015) 031005.
[25] R.F. Zhang, Z.Y. Ning, Y.Y. Zhang, Q.S. Zheng, Q. Chen, H.H. Xie, Q. Zhang, W.Z. Qian, F. Wei, Superlubricity in centimetres-long double-walled carbon nanotubes under ambient conditions, Nat. Nanotechnol. 8 (12) (2013) 912–916.
[26] W. Wang, S. Dai, X. Li, J. Yang, D.J. Srolovitz, Q. Zheng, Measurement of the cleavage energy of graphite, Nat. Commun. 6 (2015) 7853–7859.
[27] H. Zhu, S. Zhu, Z. Jia, S. Parvinian, Y. Li, O. Vaaland, L. Hu, T. Li, Anomalous scaling law of strength and toughness of cellulose nanopaper, Proc. Natl. Acad. Sci. U. S. A. 112 (29) (2015) 8971–8976.
[28] G. Anagnostopoulos, P.N. Pappas, Z. Li, I.A. Kinloch, R.J. Young, K.S. Novoselov, C.Y. Lu, N. Pugno, J. Parthenios, C. Galiotis, K. Papagelis, Mechanical stability of flexible graphene-based displays, ACS Appl. Mater. Interfaces 8 (34) (2016) 22605–22614.
[29] D. Akinwande, C.J. Brennan, Z. Li, J.S. Bunch, P. Egberts, J.R. Felts, H.J. Gao, R. Huang, J. Kim, T. Li, Y. Li, K.M. Liechti, N. Lu, H.S. Park, E.J. Reed, P. Wang, B.I. Yakobson, T. Zhang, Y.W. Zhang, Y. Zhou, Y. Zhu, A review on mechanics and mechanical properties of 2D materials—graphene and beyond, Extreme Mech. Lett. 13 (2017) 42–72.
[30] Y. Wang, R. Yang, Z.W. Shi, L.C. Zhang, D.X. Shi, E. Wang, G.Y. Zhang, Super-elastic graphene ripples for flexible strain sensors, ACS Nano 5 (5) (2011) 3645–3650.
[31] H. Jiang, D.Y. Khang, J. Song, Y. Sun, Y. Huang, J.A. Rogers, Finite deformation mechanics in buckled thin films on compliant supports, Proc. Natl. Acad. Sci. U. S. A. 104 (40) (2007) 15607–15612.
[32] V. Nayyar, K. Ravi-Chandar, R. Huang, Stretch-induced wrinkling of polyethylene thin sheets: experiments and modeling, Int. J. Solids Struct. 51 (9) (2014) 1847–1858.
[33] K. Yang, Y. Chen, F. Pan, S. Wang, Y. Ma, Q. Liu, Buckling behavior of substrate supported graphene sheets, Materials 9 (1) (2016) 32.
[34] V. Palermo, I.A. Kinloch, S. Ligi, N.M. Pugno, Nanoscale mechanics of graphene and graphene oxide in composites: a scientific and technological perspective, Adv. Mater. 28 (29) (2016) 6232–6238.
[35] Q. Zhao, H.J. Qi, T. Xie, Recent progress in shape memory polymer: new behavior, enabling materials, and mechanistic understanding, Prog. Polym. Sci. 49 (2015) 79–120.
[36] G. Anagnostopoulos, C. Androulidakis, E.N. Koukaras, G. Tsoukleri, I. Polyzos, J. Parthenios, K. Papagelis, C. Galiotis, Stress transfer mechanisms at the submicron level for graphene/polymer systems, ACS Appl. Mater. Interfaces 7 (7) (2015) 4216–4223.

# Supporting Information

## Degradation and Recovery of Graphene/Polymer Interfaces under Cyclic Mechanical Loading

*Guorui Wang[1,2], Enlai Gao[3], Zhaohe Dai[2], Luqi Liu[2,*], Zhiping Xu[3,*], Zhong Zhang[2,*]*

### S1. Coarse-grained molecular dynamics simulations

The interfacial mechanics of graphene deposited on to a PMMA substrate and its deformation occur at a characteristic length scale of tens of micrometers according to the experimental evidence. As full-atom MD simulations cannot access this length scale and the corresponding time scale, a coarse-grained molecular dynamics (CGMD) approach was pursued here. In our model, CG particles interact through bond, angle, dihedrals springs, and non-bonded interaction terms, expressed in the following forms:

$$V_b = k_b(d - d_0)^2 \quad \text{(S1)}$$

$$V_a = k_a(\theta - \theta_0)^2 \quad \text{(S2)}$$

$$V_d = k_d[1 - \cos(2\phi)]^2 \quad \text{(S3)}$$

$$V_{nb} = 4\varepsilon[(r/\sigma)^{12} - (r/\sigma)^6] \quad \text{(S4)}$$

where $k_b$, $k_a$ and $k_d$ are the spring constants of bond, angle and dihedral interaction. $d$, $\theta$ and $\phi$ are the bond length, angle, and dihedral angle, with reference values $d_0$, $\theta_0$ and $\phi_0$. Two parameters $\varepsilon$ and $\sigma$ define the energy and length scales of non-bonded interaction for the interfacial adhesion. This approach provides an energetic description that is equivalent to the continuum mechanics model with specific tensile stiffness, Poisson's ratio, bending rigidity and the adhesion between graphene and the PMMA substrate. The parameters used in our CGMD simulations are fitted to full-atom MD simulations and are listed in Table 1. [1-2]

PMMA substrate is modeled as a block with dimensions of 53 nm (length) ×4.8 nm (width) ×20 nm (height). A layer of graphene with lateral dimensions of 36 nm (length) ×4.8 nm (width) is placed at the center of the upper PMMA surface, as shown

in Figure 5a. Stretching of the system was performed in the *x* direction with periodic boundary conditions (PBC) applied in both the *x* and *y* directions, while the *z*-boundary condition is left to be open

To study the interfacial stress transfer, we first simulated cycling loading conditions with a constant strain rate at 300K, and extracted strain in graphene and the substrate, which are summarized in Figure 5b. To explore the reconstruction of graphene/PMMA interface under thermal stimuli, a three-cycle loading condition of energy minimization (0 K) was simulated where the buckles form, followed by an additional simulation with thermal stimulus introduced at 300K for 1 ns.

**Table S1.** Parameters for bonded and non-bonded interatomic potential functions used in the CG models of graphene and PMMA.

| Interaction | Parameters | |
|---|---|---|
| Bond | $d_0$ (Å) | $k_b$ |
| A-A | 2.82 | 17.54 (kcal/mol.nm$^2$) |
| A-B | 2.82 | 54.94 (kcal/mol.nm$^2$) |
| G-G | 2.8 | 460 (kcal/mol.nm$^2$) |
| Angle | $\theta_0$ (°) | $k_a$ |
| A-A-A | 131 | 3.0 kcal/mol |
| A-A-B | 71 | 10.2 kcal/mol |
| G-G-G | 120 | 409.8 kcal/mol |
| Dihedral | / | $k_d$ |
| G-G-G-G | / | 4.15 kcal/mol |
| Non-bonded | $\sigma$ (Å) | $\varepsilon$ (kcal/mol) |
| A-A | 4.25 | 0.85 |
| A-B | 4.73 | 0.65 |
| B-B | 4.73 | 0.88 |
| G-G | 3.46 | 0.82 |

*A and B are the coarsen beads in PMMA and G is the bead in graphene

**S2. Distribution of the Raman 2D-band frequency along the stretching direction**

**and surface morphology of graphene during cyclic loading**

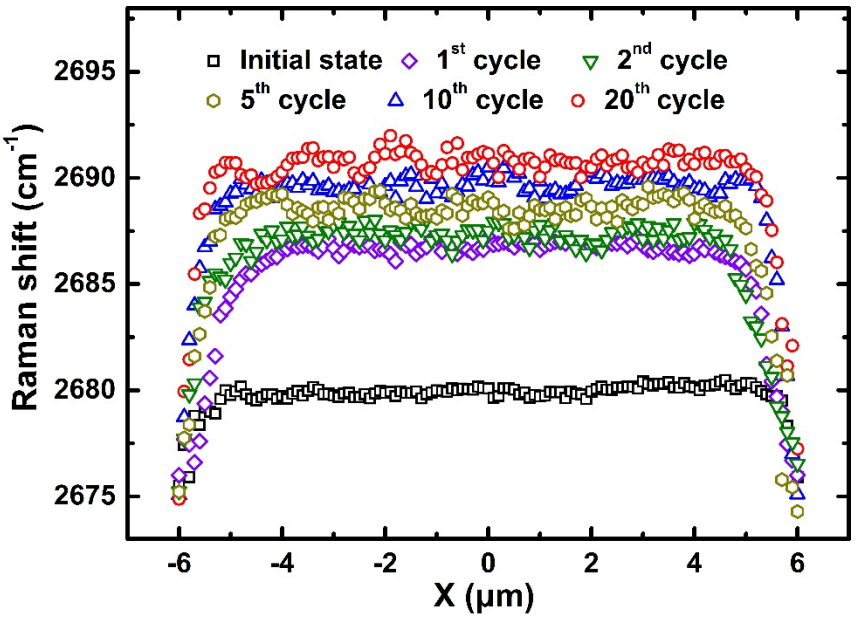


**Figure S1.** The 2D-band frequency distribution across the monolayer graphene after releasing during each loading/unloading cycle. At the initial state, graphene was under residual pre-compression throughout the sample, which might be resulted from the transfer process. [3-4] During the following loading/unloading cycles, graphene presented higher Raman frequency as it underwent interfacial sliding and subsequent compression. Moreover, the sluggish variation in Raman frequency after five cycles is also aligned with the plateau stage in the degradation of interfacial stress transfer. Note that, in the 20$^{th}$ cycle, the data points tend to be more scattered which implies the inhomogeneous strain distribution corresponding to the presence of buckles.

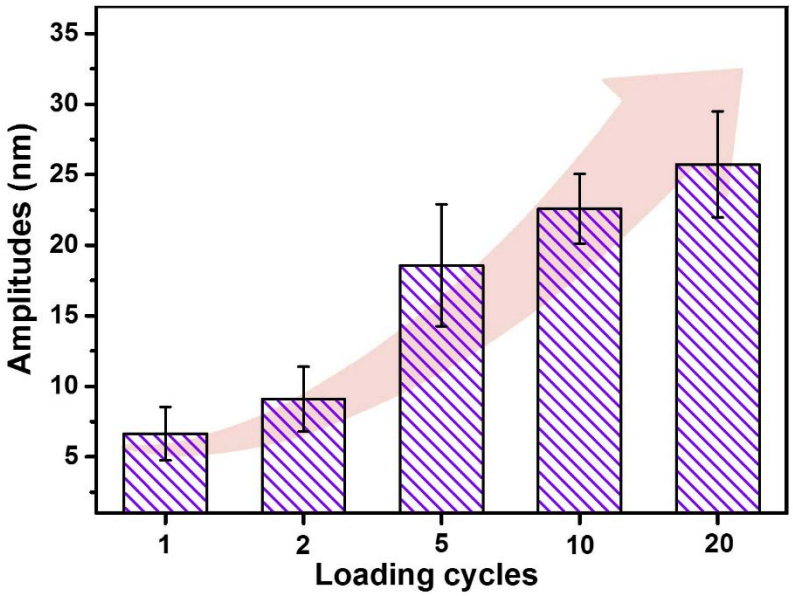


**Figure S2.** The development of buckle amplitudes during multiple loading/unloading cycles based on the AFM images from the same flake. The scattered feature of data points is attributed to the relatively lower heights extracted from the continuously emerging buckles.

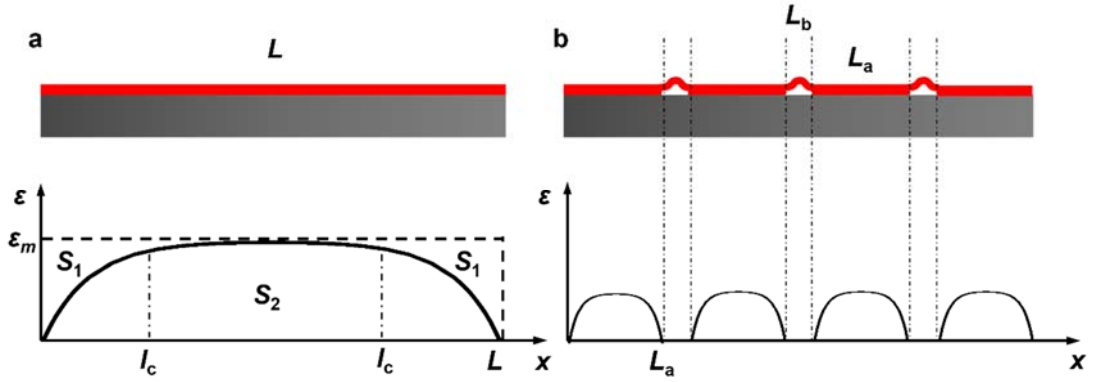


**Figure S3.** Schematic plots of strain distribution within the graphene sheet with (a) full and (b) partial contact with the substrate, respectively. $L$ is the length of graphene along the stretching direction and $\varepsilon_m$ is the top-surface strain applied to the substrate. After a few loading cycles, the contact between graphene and PMMA splits into $N$ patches, which is assumed to be in equal size for simplification. From experimental evidence, we consider the length of each patch of contact as $L_a = 1.5$ μm the lateral span of each buckle as $L_b = 0.1$ μm. In a full contact with the matrix, the graphene reinforces the matrix to the utmost extent through interfacial stress transfer, and the

distribution of in-plane strain in graphene is non-uniform. Conventionally, a critical length ($l_c$) is defined as two times the length required for the internal strain with the flake to reach 90% of that in the matrix, as presented in Figure S3a. Herein, an efficiency of stress transfer $\eta = \frac{\int_0^L \varepsilon(x)\mathrm{d}x}{\varepsilon_m L} = 1 - \frac{tanh(\beta L/2)}{\beta L/2}$ can be defined as the ratio of the integral area of $\varepsilon(x)$ ($S_2$) to the rectangular area surrounded by dashed lines and coordinate axises ($2S_1$+$S_2$), as shown in down-panel of Figure S3a. For example, for a full contact, $\eta$ is 0.80 with a typical value of $\beta L$=10, which will be reduced to $\eta = N[1 - \frac{\tanh(\beta L_a/2)}{\beta L_a/2}] = 0.55$ for the partial contact.

**S3. Raman spectra of graphene and the strain distribution in graphene during multiple loading/unloading cycles in Test II and Test III after the thermal stimulus**

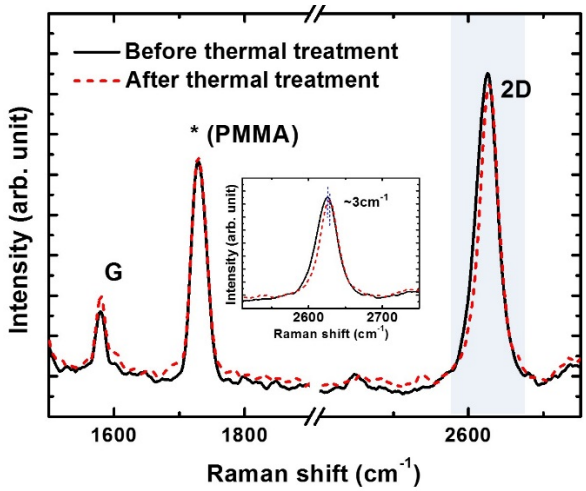


**Figure S4.** The Raman spectra of graphene before and after thermal treatment. The inset presents the variation of Raman 2D-band (3 $cm^{-1}$), corresponding to a negligible strain of ~0.06%.

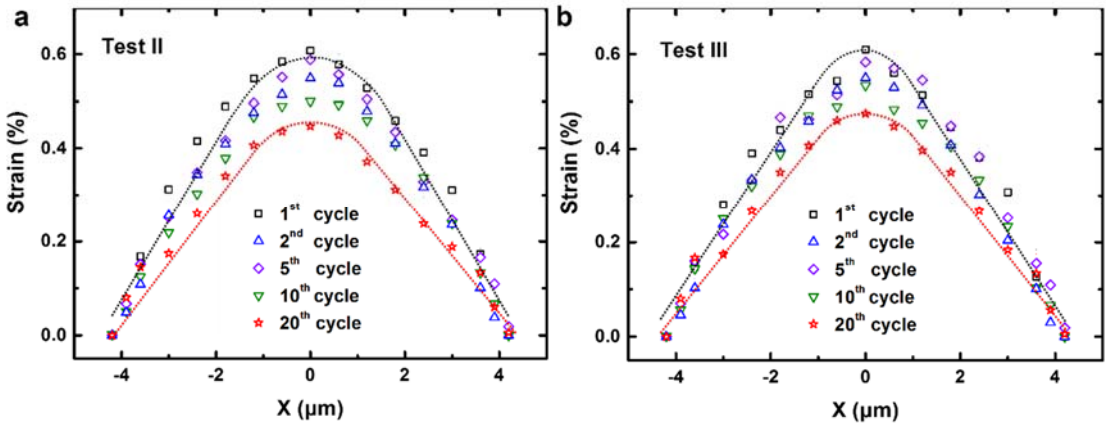


**Figure S5.** Strain distribution in graphene along the direction of tension at the averaged strain level of 0.7% during multiple loading/unloading cycles in Test II and Test III, respectively.

## References

1. Ruiz, L.; Xia, W.; Meng, Z.; Keten, S., A Coarse-grained Model for the Mechanical Behavior of Multi-layer graphene. Carbon 2015, *82*, 103-115.

2. Uttarwar, R. G.; Potoff, J.; Huang, Y., Study on Interfacial Interaction between Polymer and Nanoparticle in a Nanocoating Matrix: A MARTINI Coarse-graining Method. Ind. Eng. Chem. Res. 2012, 52(1), 73-82.

3. Frank, O.; Tsoukleri, G.; Parthenios, J.; Papagelis, K.; Riaz, I.; Jalil, R.; Novoselov, K. S.; Galiotis, C., Compression Behavior of Single-layer Graphenes. ACS Nano 2010, *4* (6), 3131-3138.

4. Anagnostopoulos, G.; Androulidakis, C.; Koukaras, E. N.; Tsoukleri, G.; Polyzos, I.; Parthenios, J.; Papagelis, K.; Galiotis, C., Stress Transfer Mechanisms at the Submicron Level for Graphene/Polymer Systems. ACS Appl. Mater. Interfaces, 2015, 7(7), 4216-4223.